ORIGINAL ARTICLE

Challenges of nanoparticle-reinforced NiAl-based coatings processed by in situ synthesis of the aluminide

Heber O. Abreu-Castillo[1] · Ana Sofia C. M. d'Oliveira[2]

Abstract

NiAl intermetallic-based hardfacing coatings were processed by *in situ* synthesis from elemental Ni and Al powders mixtures, by Directed Energy Deposition - Plasma Transferred Arc (DED-PTA). The exothermic nature of NiAl synthesis promotes the formation of columnar grains, which do not contribute to mitigate the low toughness of the material at room temperature, limiting its use. Refining the microstructure is a path to overcome this limitation and the approach used took advantage of tungsten carbide nanoparticles (WC-NPs) to limit grain growth during solidification. During preparation of powder mixtures, the adhesion of 1 wt.%WC-NPs to the surface of Ni particles (which act as carriers) helps to reduce the tendency to agglomeration. However, this approach proved to be ineffective for the *in situ* synthesis of NiAl, since the NPs form a film of molten material on the Ni particle surface as they cross the plasma arc, limiting the interdiffusion of Ni and Al, compromising the synthesis of the aluminide alloy. The present study assessed this challenge by investigating the amount of NP carriers, i.e, the proportion of Ni particles that carry the NPs, that allows both for the synthesis of NiAl, and grain refining due to the WC-NPs. Results show that β-NiAl phase was successfully formed in multi-layer coatings, processed *in situ* by DED-PTA. Powder mixtures containing 50% and 70% NP carriers promoted a progressive reduction in grain size by the addition of 1 wt.% WC-NPs in the Ni+Al powder mixture, followed by an increase in hardness.

Keywords Ni aluminides · Multi-layers · Intermetallics · Plasma Transferred Arc · Grain refinement · Nanoparticles

1 Introduction

Nickel aluminide (NiAl) alloys have been widely studied and applied in the energy, manufacturing, automotive, and aerospace industries. The attractiveness of the aluminide compounds for high-temperature applications is a consequence of their ordered structure and high melting point (1640 °C), which is 100–250 °C higher than conventional Ni-based superalloys, thermal stability, relatively low density (5.9 g/cm^3) compared with advance superalloys with 8.60 g/cm^3, satisfactory corrosion resistance, good thermal conductivity (76.0 W/m.K), and resistance to oxidation, which is characterized by the formation of an adherent and protective Al_2O_3 scale, with a growth rate that is controlled by relatively slow diffusion of oxygen [1–4]. However, the NiAl has poor fracture toughness at room temperature making processing and handling of alloys a challenge. Efforts have been directed towards using NiAl in thermal barrier coatings to protect nickel superalloys as a bond layer on which the top layer of a ceramic material is deposited, offering high oxidation resistance together with an increase in thermal expansion compatibility with the substrate [5, 6].

Different approaches have been adopted to improve the toughness of brittle materials. In general, they can be divided into two types of toughening: extrinsic and intrinsic. In extrinsic toughening, the main characteristic is the incorporation of ductile phases or fibers to reduce the stress at the cracks. Intrinsic toughening, the aim is to provide resistance to crack growth by reducing grain size [7]. Grain refinement is a conventional approach, commonly used for improving the ductility and toughness of metallic alloys [3] although a different response is found in intermetallic alloys.

Refining the microstructure of NiAl alloys can help to improve room-temperature toughness and yield strength. Schulson and Barker [8] demonstrated that grain refinement

✉ Ana Sofia C. M. d'Oliveira
sofmat@ufpr.br

1 Materials Science and Engineering Post-Graduation Program, Universidade Federal do Paraná, Curitiba, Brazil

2 Mechanical Engineering Department, Universidade Federal do Paraná, Curitiba, PR, Brazil

below a critical value (20 μm) exhibited considerable improvements in ductility, increasing 8% and 40% tensile elongation for 20 μm and 8 μm grain size, respectively. Also, it was observed that the yield strength, microhardness, and fracture strength obey the Hall-Petch relationship, confirming that mechanical properties improve with a refinement of the grain size [3, 9]. In summary, grain refinement can enhance toughness offering a larger crack propagation resistance that accounts for the increase in elongation, yield, and fracture strength simultaneously. The oxidation rate of NiAl can also be reduced by grain refinement, as demonstrated by Kaplin [10].

Aiming to refine microstructure of metallic alloys, additions of micro and nanoparticles have been carried out including NiAl, SiC, TaC, Al_2O_3, TiB_2, NbC, ZrB_2, and TiC [11–14]. In a NiAl matrix, WC has been shown to be the most effective, due to its high friction resistance, high melting point, and strength and low solubility in this intermetallic [15]. These finer microstructure composite alloys have been processed through different techniques, among which self-propagating high-temperature synthesis (SHS), hot isostatic pressing (HIP), spark plasma sintering (SPS), mechanical alloying (MA), and directional solidification (DS) [14].

Nanoparticles (with sizes between 1 and 100 nm) have been successfully added to refine the microstructure of steels, Co and Ni superalloy-based coatings, processed through the deposition of powder mixtures with Plasma Transferred Arc Directed Energy Deposition (PTA-DED), improving microhardness and wear resistance [16, 17]. PTA-DED is a hardfacing process, commonly used globally and adapted to fabricate large parts by additive manufacturing. PTA-DED starts when a pilot arc is ignited between non-consumable W electrode and the torch following by the main arc that consists in an ionized argon gas that forms a plasma arc column (formed between a torch and the substrate) that works as a heat source, when argon gas passes through an inner ring between the cathode and anode [18, 19]. Powder mixtures or alloys are fed into plasma arc, melted, and deposited on a molten pool in the substrate, promoting a metallurgical bonding substrate/coating.

Claros and collaborators [16] used WC-NPs to process WC/Ni-based nanocomposites by PTA-DED (powder feedstock). Authors report that the dispersion of nanoparticles requires special procedures to prepare the powder mixture to avoid agglomeration of NPs. Due to their high surface-to-volume ratio that accounts for a high surface energy, the distribution of NPs in the matrix is impacted, reducing the effectiveness of the reinforcement. To overcome this behavior, WC-NPs were impregned on the Ni-based alloy particles, which worked as "carriers" of the NPs during deposition. The authors report the procedure to be effective regarding the dispersion of WC nanoparticles in coatings, obtaining a good distribution in the matrix, reduction of particle agglomeration, prevention of microcracks propagation, and an improvement in the wear behavior.

Acevedo-Davila [17] and Bond [20] also, report the incorporation of NPs during the preparation of powders to process Co-based nanocomposites by PTA-DED achieving a good distribution of NPs and grain refinement. Prass et al. [21] also used Claros et al.'s approach in the preparation of the powder mixtures, to incorporate either Cu or CuO nanoparticles in a AISI 316L stainless steel matrix nanocomposites. Authors report that the PTA-DED multilayers exhibited a good distribution of the nanoparticles and grain refinement.

The PTA-DED processing of NiAl-based coatings via in situ synthesis has some particularities compared to coatings processed with commercial alloy powders. Ni+Al elemental powder mixtures are prepared and fed into a plasma arc (PTA torch), where the particles are melted and the interdiffusion of elements starts, promoting the synthesis of this intermetallic compound in situ [22]. Other authors have demonstrated the effectiveness of this procedure to obtain NiAl-based coatings on AISI 1020 carbon steel [23] and AISI 304 stainless steel substrates [24].

The previous work has shown that modification of the Ni+Al powder mixtures with WC nanoparticles (WC-NPs) to compromise in situ synthesis of aluminide coatings [22]. Authors used the Ni particles in the Ni+Al powder mixture as carriers of the WC-NPs and identified that the interdiffusion of elements in the plasma arc required for the successful synthesis of aluminide alloys was hindered. Researchers discuss that two phenomena occurring in the plasma arc account for the observed behavior: WC-NPs impregnated on the surface of Ni powders in the Ni+Al powder mixture, form a liquid film surrounding Ni particles, compromising the necessary interdiffusion between molten Ni and Al particles during deposition, inducing a more significant loss of aluminum as it melts and vaporizes in the plasma arc, accounting for the formation of Ni-rich aluminides, such as Ni_3Al [22].

The present work brings an important contribution to the processing of β-NiAl-based coating while taking advantage of the effects of a dispersion of WC-NPs in the matrix. To overcome the reported limitations a novel approach was used where only a fraction of the Ni powder in the Ni+Al powder mixture is used as NPs carriers. This procedure should allow enough Ni to react with Al powder in the plasma arc promoting the synthesis of NiAl and mitigating the loss of Al while incorporating the WC-NPs in coatings. This study assesses the impact of the configuration of Ni+Al powder mixtures on coatings, focusing on the synthesis of β-NiAl and how its amount and distribution impact the microstructure morphology and microhardness.

The developed procedures represent an important advance in the availability of a variety of intermetallic alloys obtained by in situ processing offering opportunities for their use as coatings or functionally graded materials (FGMs), in which chemical composition and microstructure can be controlled, inducing gradual changes in the mechanical properties and oxidation resistance in a single piece.
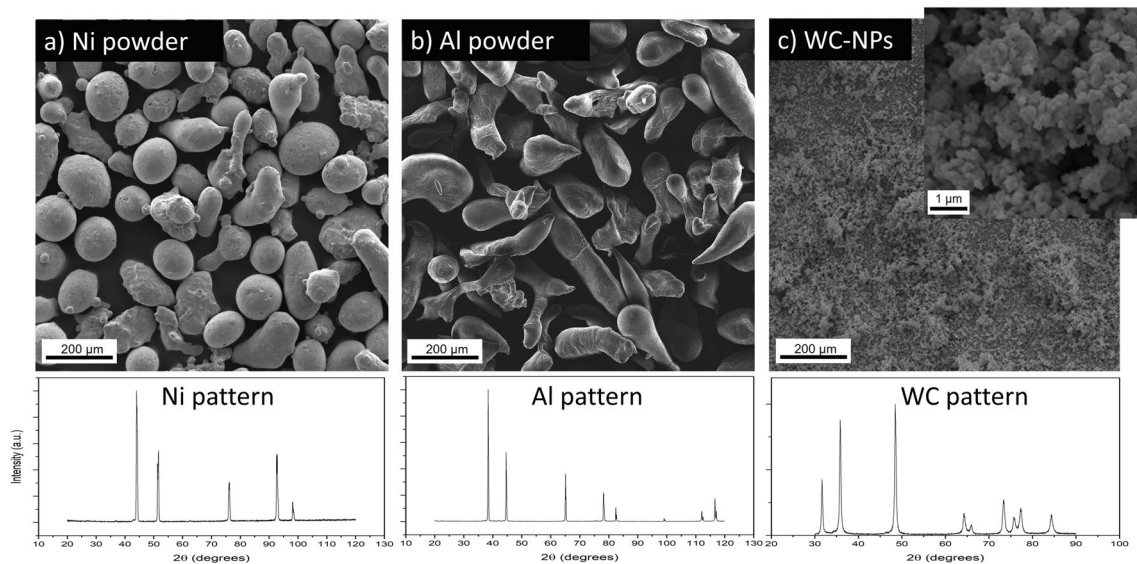
Fig. 1 Elemental Ni and Al powders and tungsten carbide nanoparticles. **a** Ni powder; **b** Al powder; **c** WC nanoparticles

2 Materials and processing

Non-spherical Ni and Al powders, 99.9% purity, with grain size ranging from 75 to 150 μm were used (Fig. 1). Tungsten carbide nanoparticles (WC-NPs) with an average particle size of 55 nm were used as reinforcing particles (Fig. 1 and Table 1). Four different powder mixtures were prepared (C-0, C-50, C-70, and C-90), containing Ni+Al elemental particles, with and without 1 wt.% tungsten carbide nanoparticles (WC-NPs), according to Table 2. The Ni/Al ratio (wt.%) is 4.0 for all of the prepared powder mixtures.

The reduced size of the nanoparticles results in a high surface energy and consequently a strong tendency for

agglomeration (clustering), which compromises a good homogenization of powders distribution [16, 20]. To mitigate this effect, nanoparticles were impregnated on the surface of the Ni particles by using its surface energy [16]. The fraction of Ni particles that carry the nanoparticles impregned on its surface (Ni+WC-NPs) is referred to as "carriers."

The fraction of carriers used is 50, 70, and 90% of the Ni in the Ni+Al powder mixtures referred to as C-50, C-70, and C-90 powder mixtures, respectively (Table 2). The C-0 powder mixture does not contain WC-NP additions. Table 2 shows the composition of the powder mixtures, the fraction of carriers, and the Ni fraction left without nanoparticles. The prepared powder mixtures are illustrated in Fig. 2 showing a representation of the fraction of Ni+WC-NPs (carriers) and Ni particles without NPs in each powder mixture. With this approach, it is expected the fraction of Ni particles without NPs to react with aluminum igniting the synthesis of NiAl compound in the plasma arc.

The preparation of the carriers and the powder mixtures consists of five steps, extrapolating procedures described by Molina-Claros et al. [16], as follows:

Table 1 Elemental powders and WC-NPs

Powder	Size	Purity (%)
Ni	75 to 150 μm	99.9
Al	75 to 150 μm	99.9
WC nanoparticles (WC-NPs)	55 nm	99.9

Table 2 Powder mixture compositions

Powder mixture/ coating	Composition (wt.%)	Fraction of carriers (%)	Fraction of Ni without NPs (%)
C-0	(80 Ni - 20 Al)	0	100
C-50	(39.6 Ni – 1 WC-NPs) + (39.6 Ni – 19.8 Al)	50	50
C-70	(55.44 Ni – 1 WC-NPs) + (23.76 Ni – 19.8 Al)	70	30
C-90	(71.28 Ni – 1 WC-NPs) + (7.92 Ni – 19.8 Al)	90	10

Fig. 2 Representation of the powder mixtures used in the present work. **a** C-0 powder mixture; **b** C-50 powder mixture; **c** C-70 powder mixture; **d** C-90 powder mixture
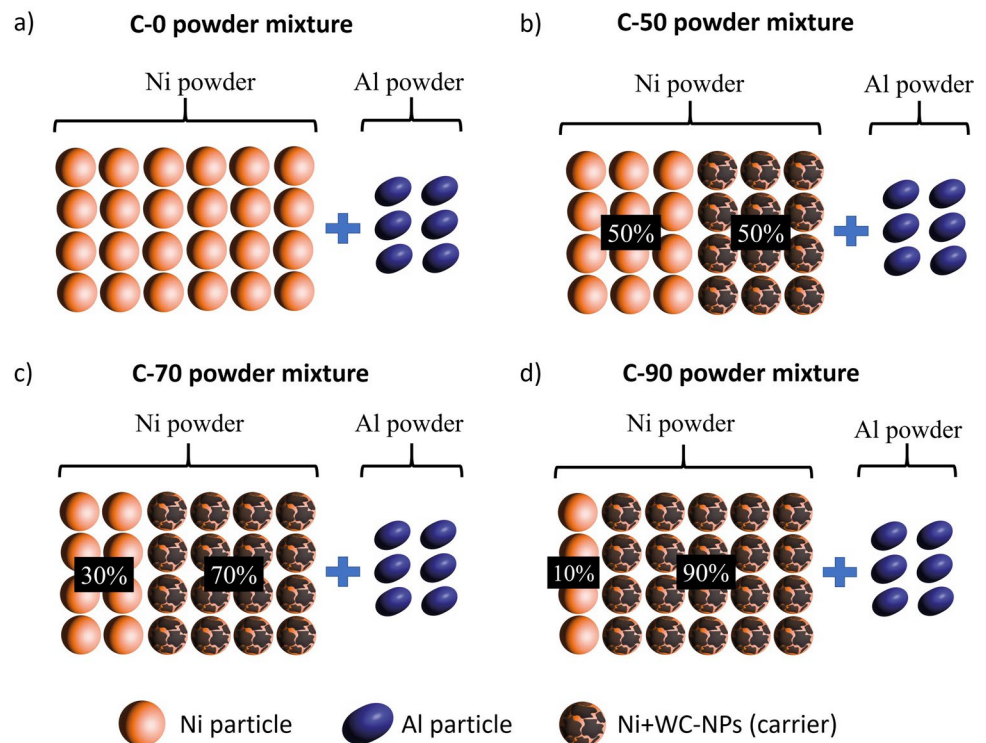
1. The WC nanoparticles were weighed and dispersed in absolute alcohol in an ultrasound bath for 90 min.
2. A fraction of Ni powder was added and magnetically stirred for 90 min to improve the impregnation of the nanoparticles on the surface of the Ni grains (Ni+WC-NPs mixture).
3. The Ni+WC-NPs mixture was put again in the ultrasound bath for another 90 min.
4. The Ni+WC-NPs mixture is dried in a drying furnace at 50 °C, until the absolute alcohol is completely vaporized.
5. Finally, the rest of Ni powder without NPs is added, together with the Al powder, and homogenized in a "Y" mixer for 02 h at 12 RPM.

Figure 3 shows a Ni particle without and with WC-NPs impregnated on its surface.

Four single-layer coatings were processed by using each of the powder mixtures prepared. The coatings were processed by PTA-DED, by using a Starweld 300M hardfacing system equipped with a torch Model 600. A fixed set of deposition parameters was used (Table 3). These deposition parameters were chosen based on a previous work [22–24].

In PTA-DED, powder mixtures are transported through the torch by using a powder carrier gas (argon) and exit at orifices on the anode face, intersecting the plasma column at a distance above the substrate [18] (Fig. 4a). The powder is introduced into a weld pool that forms on the substrate surface (Fig. 4b). The weld pool is protected from oxidation by a shielding gas that flows from an outer annulus in the torch [18]. The processed coating is characterized by a metallurgical bond between coating and substrate.

All the depositions were carried out on stainless steel plates of AISI 304 (150 mm × 100 mm × 10 mm). The chemical composition of the substrates used is shown in Table 4. One hundred millimetre length single-layer coatings were deposited in a preheated substrate (200 °C) to better control the cooling rate and avoid cracks [22].

Optical macro images of the transversal cross-section of the coatings were obtained with a stereoscopic microscope by using a ×2.25 magnification. The microstructural characterization of coatings used scanning electron microscopy (SEM), with a back-scattered electron detector (BSE) on different regions of the cross-section of the coatings, at approximately 0.6 mm from the top. Quantitative analysis of the volume fraction of the phases in the coatings was carried out by using image analysis through EDAX OIM Analysis Software, on a minimum of three regions at approximately 0.6 mm from the top. The volume fraction average for each phase was calculated.

The impact of the interaction with the austenitic stainless-steel substrate was assessed by dilution, as the ratio of iron was calculated through Eq. 1 [25, 26]. The iron content was assessed by energy dispersive spectroscopy (EDS), on the coatings ($Fe_{coating}$, wt.%) and on the substrate ($Fe_{substrate}$, wt.%). This EDS analysis was carried out on a 200×200 μm^2 area, at approximately 0.6 mm measured from the top of the coatings. A minimum of three different EDS spectra

Fig. 3 SEM image of a Ni particle **a** without NPs; **b** Ni particle with NPs impregnated on the surface (carrier)
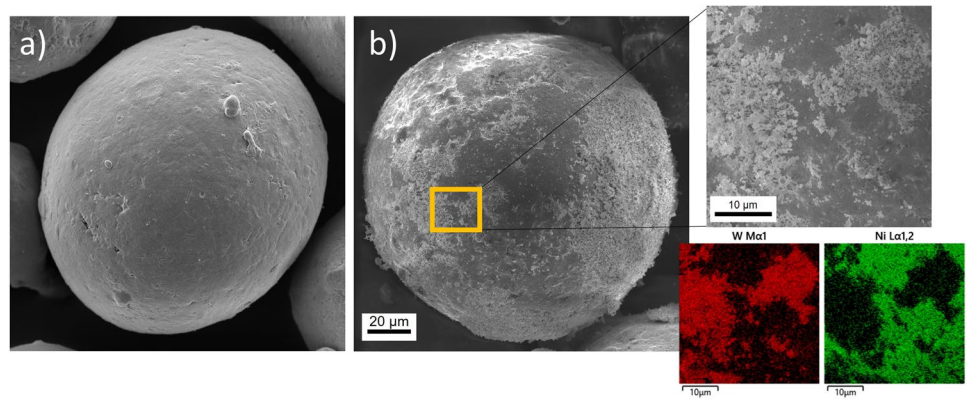

Table 3 PTA-DED processing parameters

Deposition current	Deposition speed	Powder feed rate	Stand-off distance	Plasma gas	Shielding gas	Powder carrier gas	Number of layers
100 A	100 mm/min	6.0 g/min	10 mm	2 L/min (argon)	15 L/min (argon)	0.8 L/min (argon)	1

Fig. 4 The PTA-DED processing. **a** Graphic representation of PTA-DED torch; **b** deposition of a coating through the use of powder mixtures
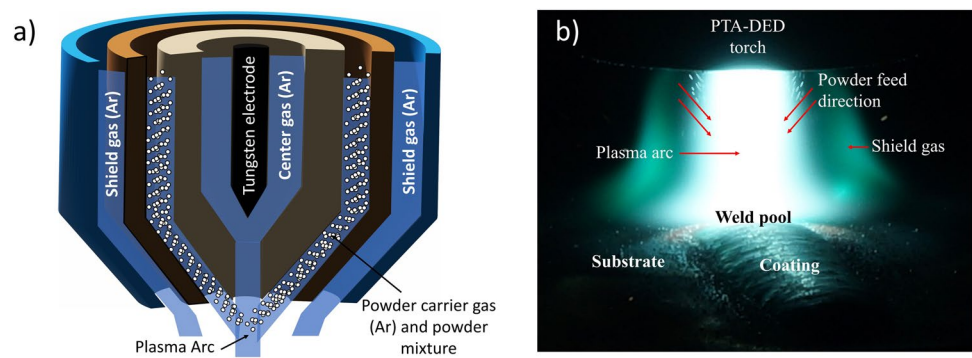
Table 4 Chemical composition of AISI 304 stainless steel substrate (wt.%)

Fe	Cr	Ni	Mn	Si	C	Others
Bal.	18.35	7.84	1.13	0.40	0.07	2.58

were measured for $Fe_{coating}$ and $Fe_{substrate}$, respectively, and the average values were calculated.

$$\text{Dilution (\%)} = \frac{Fe_{coating}}{Fe_{substrate}} \times 100 \qquad (1)$$

Vickers microhardness was measured on the cross-section of coatings (Fig. 5a), under a 2.942 N load (0.3 kgf), after metallographic procedures. For this, the cross-section of the coatings was grounded (up to 1200 grit sandpaper) and polished with alumina polishing suspension (1 µm). The surfaces were cleaned in an ultrasonic cleaning bath. Three indentations profiles, 200 µm spaced apart, were measured.

A minimum of 36 indentations were used to determine the average microhardness of each coating.

X-ray diffraction analysis was performed on the top surface of the coatings (Fig. 5b) to identify the phases, using Cu kα radiation ($\lambda = 0.15406$ nm), at 1.0 degrees/min scan speed, from 30 to 120° (2θ) for a general analysis. For a more specific analysis of the main peaks of the phases, this scanning was performed at 0.1 degrees/min scan speed from 42.5 to 45.5°(2θ). Prior to this analysis, the top surfaces of the coatings were grounded (up to 1200 grit sandpaper) and polished with alumina polishing suspension (1 µm). The surfaces were cleaned by an ultrasonic cleaning bath before X-ray diffraction analysis.

Fig. 5 Characterization of the coatings. **a** Indentation of the Vickers microhardness test; **b** top surface used for XRD analysis
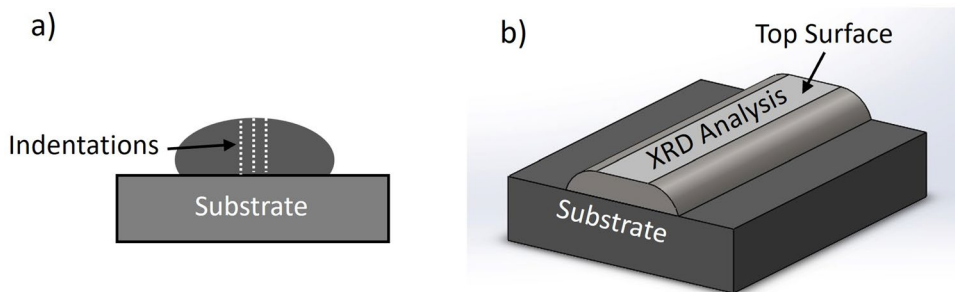
Microstructural analysis was complemented with electron backscatter diffraction (EBSD) with a ×300 magnification in order to reveal the shape and size of the grains. All the EBSD images were taken at approximately the same distance from the top (0.6 mm from the top of the coatings). Grain sizes were measured using the linear intercept method. For this, a minimum of three microstructural images (×300 magnification) with ten randomly oriented lines each, aiming to obtain the average of this measurement.

3 Results and discussion

The impact of the amount of Ni particles in the Ni+Al powder mixture used as carriers to the WC-NPs in the in situ synthesis of β-NiAl and the effectiveness of the powder mixture for the four processed compositions, C-0, C-50, C-70, and C-90 are characterized, regarding coatings composition, microstructure, and hardness. Considering that the amount of nanoparticle carriers varied from 50%, 70%, to 90% of Ni, significant changes associated with these different configurations are expected.

Sound and crack-free coatings were obtained for all processed compositions, as confirmed by deep dye testing. The optical macro images of the cross-section of coatings processed with prepared powder mixtures are shown in Fig. 6.

The in situ synthesis of β-NiAl and other phases in coatings are shown in Fig. 7, as identified by X-ray diffraction analysis. β-NiAl phase together with the austenitic γ-(Fe, Ni) phase are present in coatings processed with the Ni+Al powder mixture without WC-NPs (C-0 coating), Ni+Al containing WC-NPs adhered on 50 and 70% of the Ni available (C-50 and C-70 coatings, respectively). However, coatings processed with the Ni+Al powder mixture containing WC-NPs adhered on 90% of the Ni particles (C-90 coating) showed both β-NiAl and γ'-Ni₃Al phases without the austenitic γ-(Fe, Ni) phase.

The main peaks of X-ray diffraction analysis for β-NiAl are shown in Fig. 7b. β-NiAl peaks exhibit a slight and progressive shift to the left, starting from the position of the C-0 coating, then the C-50, and finally the C-70 coating.

These changes can be better observed in Table 5, that shows the diffraction angle (2θ) associated to β-NiAl main peak and the specific stoichiometry of each phase. This shift is associated with small changes in the stoichiometry of the NiAl compound that formed in each coating, due to the wide solubility range of β-NiAl phase (41–67 at.% Ni), as shown in the Ni-Al binary phase diagram [27]. Only the C-90 coating showed a shift of the β-NiAl main peak to the right side, which is associated to the presence of Al-rich aluminide [22].

Figure 8 shows the microstructure of the processed coatings. C-0, C-50, and C-70 coatings exhibit β-NiAl dendrites (dark grey) surrounded by γ-(Fe, Ni) phase on the interdendritic region (light grey), showing that the first phase to form is the NiAl confirming the strong interaction between Ni and Al powders, in spite of the significant amount of Ni particles acting as carriers of NPs. However, when the interaction in the plasma arc between Ni and Al particles is compromised (C-90 coating), γ'-Ni₃Al dendrites (light grey) dorm, while β-NiAl remains on the interdendritic region (dark grey), Fig. 8d.

The presence of β-NiAl and γ-(Fe, Ni) phases on the C-0 coating is expected, as shown in the works by Abreu-Castillo et al. [22], Almeida et al. [23] and Brunetti et al. [24]. The B2-structured β-NiAl phase is formed due to the availability of elemental Ni and Al in the powder mixture and a suitable interdiffusion among them during deposition [22]. This suggests that the *in situ* synthesis of β-NiAl was not compromised by the addition of the WC-NPs to the Ni+Al powder mixtures used for C-50 and C-70 coatings.

Iron element, diffusing from the substrate, is known to have high solubility in the NiAl compound [28], and can lead to the formation of complex intermetallic compounds in the Ni-Al-Fe system. The substitutional solid solution NiAl(Fe) is characterized by Fe atoms replacing both Ni and Al in the B2-NiAl crystal lattice. Consequently, the formation of Fe-rich structures such as [Fe, Al]Ni (where Fe atoms occupy positions in the Ni sub-lattice) and Al[Ni, Fe] (where Fe atoms occupy positions in the Al sub-lattice) is likely [29]. This substitutional dynamic accounts for the formation and increase in density of point defects
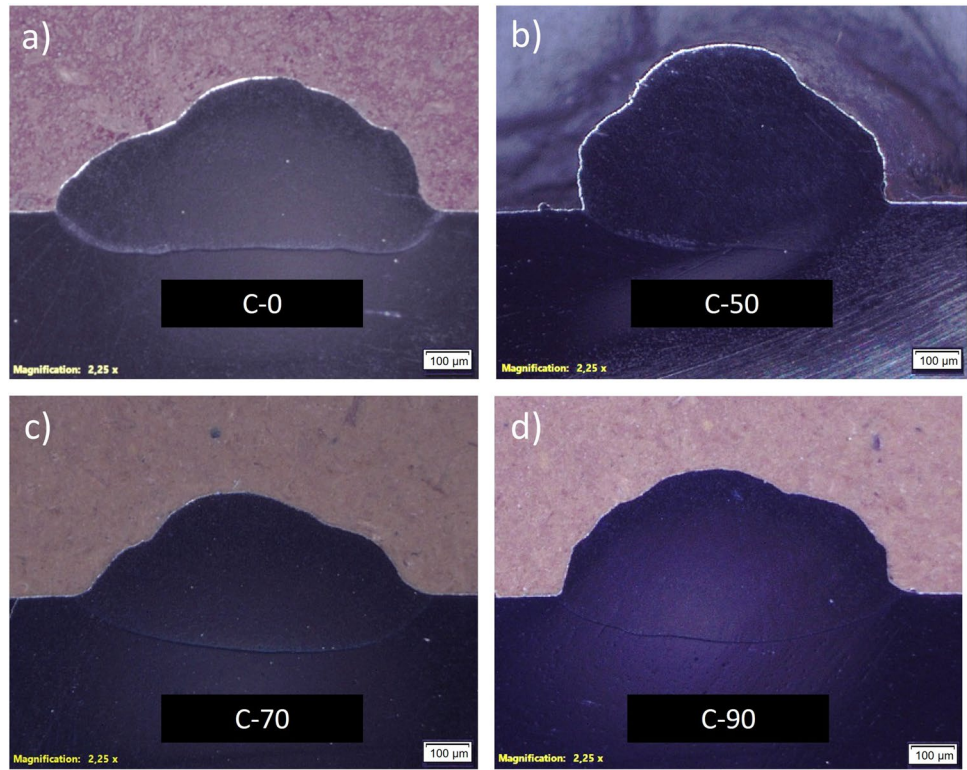
Fig. 6 Transversal cross-section of the coatings

Fig. 7 X-ray diffraction analysis of the coatings. **a** XRD diffractogram; **b** detail of the main peaks
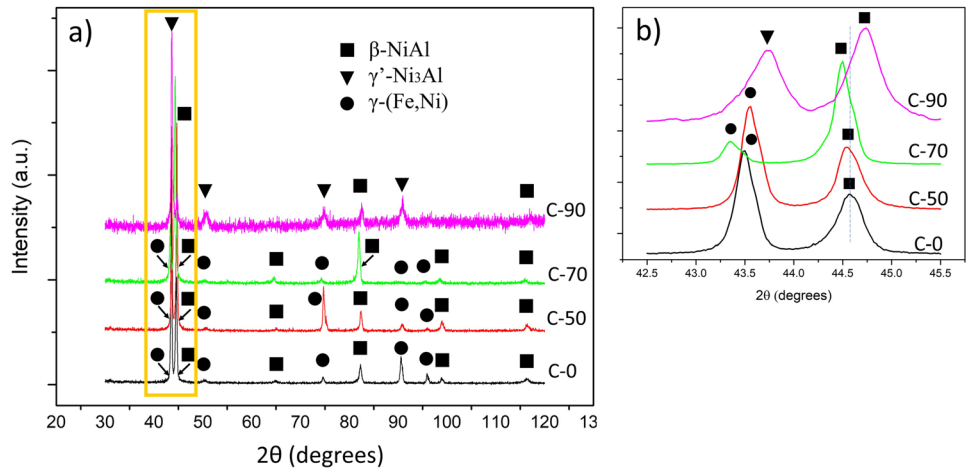

Table 5 2θ angle of β-NiAl main peaks

Coatings	2θ main peak (β-NiAl phase)	Phase
C-1	44.58	Al0.9Ni1.1
C-50	44.56	Al0.9Ni1.1
C-70	44.50	Al0.96Ni1.04
C-90	44.74	Al1.1Ni0.9

such as vacancies (present in Al-rich compounds) and Ni anti-sites (present in Ni-rich compounds), with strong effects in the mechanical properties [22].

Although the main elements in the coatings are Ni, Al, and Fe, no iron aluminides were found in the XRD analysis. This behavior can be accounted for by the enthalpy of the formation of iron aluminides (Fe-Al system) ranging from −27.15 to −36.29 kJ/mol [30], which is relatively low
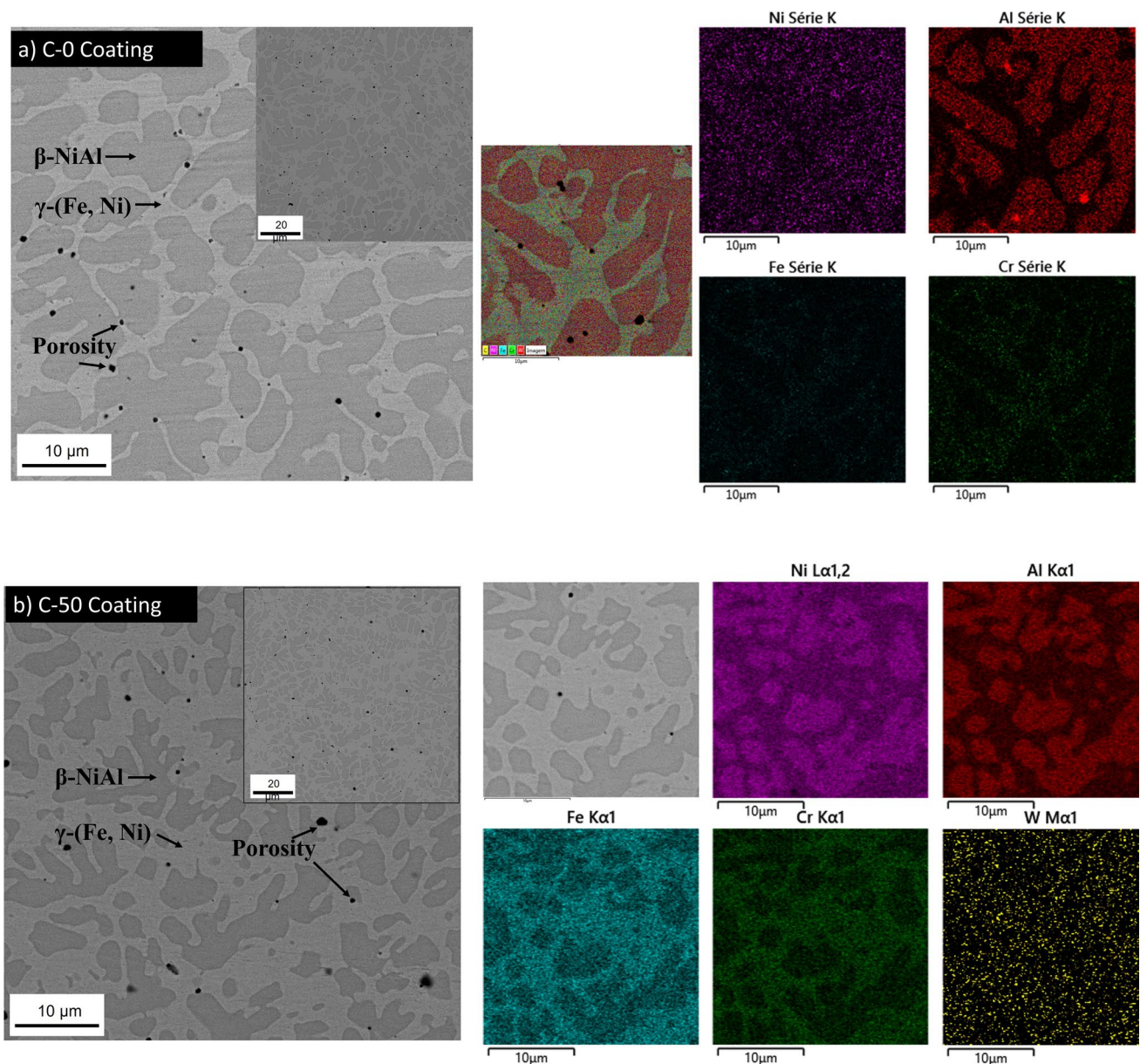
Fig. 8 Microstructure of the coatings and EDS mapping. **a** C-0 coating; **b** C-50 coating; **c** C-70 coating; **d** C-90 coating

compared to that of NiAl and inducing the preferential formation of the Ni aluminide.

WC peaks due to agglomeration or precipitation of WC particles were not found in the XRD analysis and microstructure (Figs. 7 and 8). The low solubility of W in the NiAl (ranging from 0.4 to 1 at.% [22]) allows us to predict that it was diluted in both phases in coatings due to the low amount of nanoparticles added. Compositional EDS maps in Fig. 8 show a uniform distribution of W in the microstructure, with a slightly tendence to the interdendritic regions, together with the γ-(Fe, Ni) phase.

The austenitic γ-(Fe, Ni) phase formed due to the interaction with the austenitic stainless-steel substrate (AISI 304),

is expected in coatings with iron content above 22.8 wt.%, [24], in agreement with phases identified in C-0, C-50, and C-70 coatings. Iron can be present in the powder mixtures or diffuse from the substrate as a consequence of dilution as is the case in this study. Chromium diffusing from the stainless steel substrate has low solubility in NiAl, but when present, it has preference for the Al lattice, leading to the formation of Cr-rich compounds such as [Al, Cr][Fe, Ni], with Cr atoms occupying positions in the Al sub-lattice. Hence, Cr atoms are expected to be better accommodated γ-(Fe, Ni) phase instead of β-NiAl phase, as seen in Fig. 8.

In C-90 coatings both aluminides form β-NiAl and γ'-Ni$_3$Al. The latter is expected when processing powder
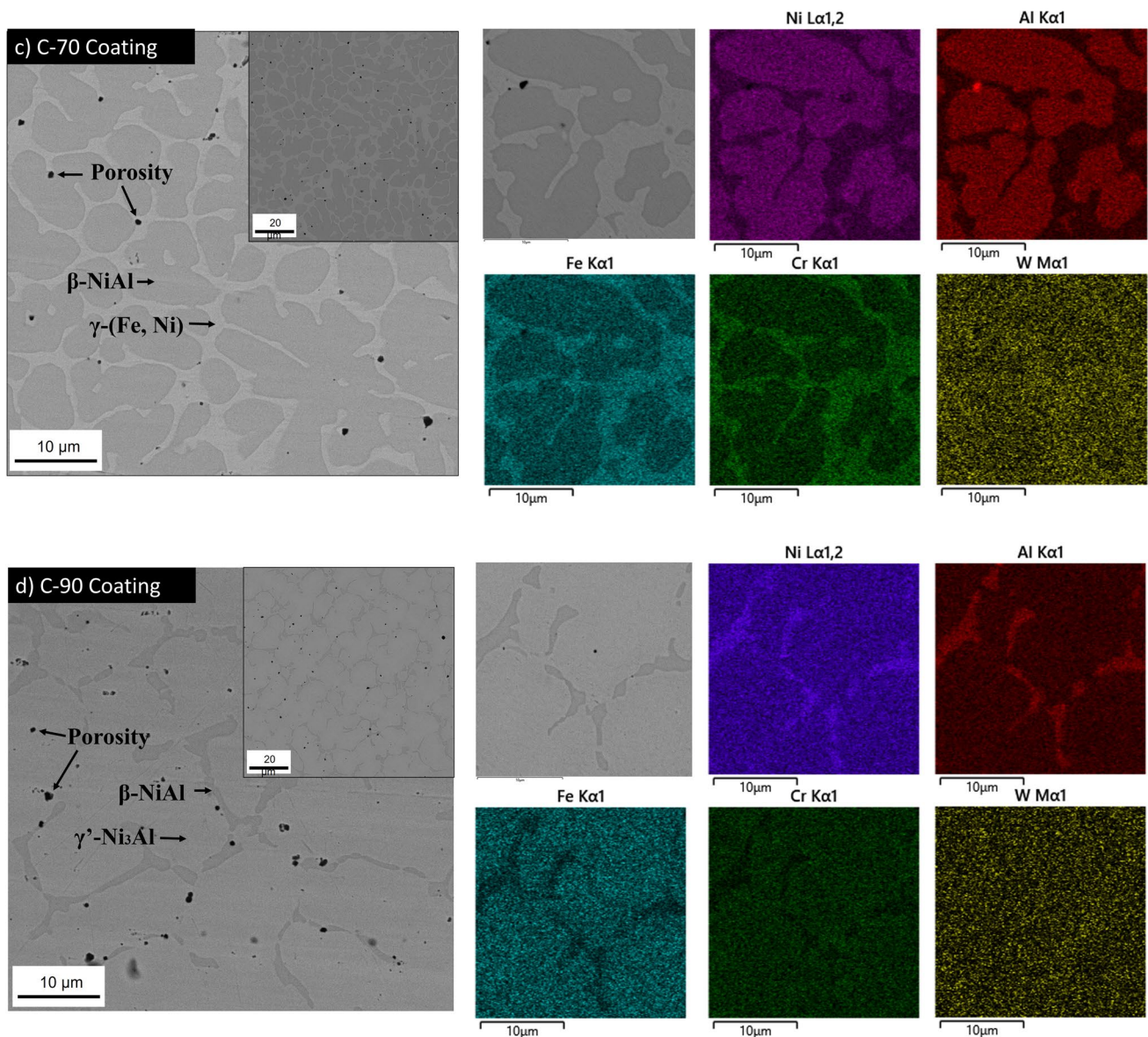
Fig. 8 (continued)

mixtures with a lower content of Al [23] and agrees with the hypothesis of a more significant loss of aluminum in the plasma arc during the processing by PTA-DED. The synthesis of a large volume of the Ni-rich aluminide, γ'-Ni₃Al, also explains the stoichiometry of the β-NiAl (Table 2).

Dilution, defined as the contribution of the composition of substrate to the deposited coating [26], as shown in Fig. 9. The dilution of the processed coatings is in a range between 29 and 45% (Fe-content method), which is relatively high compared to that expected in superalloy coatings, whose values are in the range of 5–30% (calculated through geometrical method) [18, 25].

High levels of dilution are typical of NiAl-based coatings processed, via *in situ* synthesis, with the same deposition

parameters as in the present work. Literature reports dilution values to depend on the substrate steel and processing parameters used: Almeida et al. [23] determined dilution in the range of 39–51%, by using AISI 1020 substrates, Abreu-Castillo et al. [22] 42%, on AISI 304 substrate and Brunetti et al. 30%, on AISI 304 substrate [24].

High levels of dilution in NiAl-based coatings result from a rapid solidification of the deposited material, that allow for a strong direct impact of the plasma arc on the substrate [23], together with the highly exothermic formation of the NiAl intermetallic compound (the heat of formation of NiAl is −72 kJ/mol at the stoichiometric composition [3]), indicating that a significant amount of heat is released at the solidification front in the melt pool. Breuer
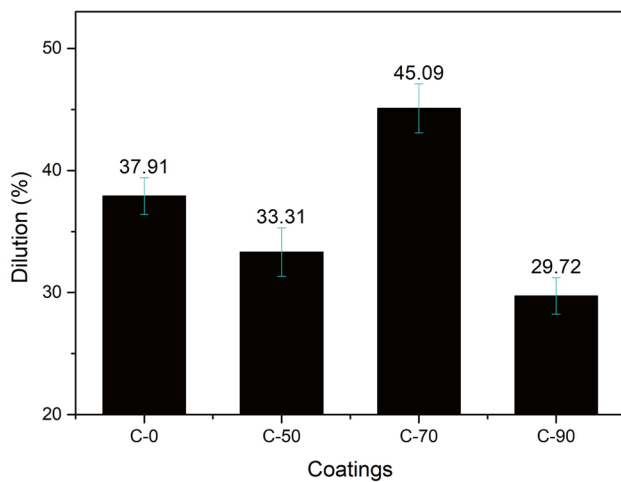
Fig. 9 Dilution of the coatings

et al. [30] showed that the enthalpy of formation of solid B2- $(Fe,Ni)_{1-x} Al_x$ varies in a range between −39.85 and −65.38 kJ/mol, being this maximum value for low-iron content and near-stoichiometric aluminides ($Ni_{0.55} Al_{0.45}$). The solidification characteristics during PTA-DED and synthesis of aluminides are therefore expected to facilitate the diffusion of elements from the substrate into the coatings (dilution) [22].

The thermal conductivity (K) of the substrate and the deposition current used during the processing can also play a significant role on the dilution levels of coatings: the low thermal conductivity of AISI 304 stainless steel substrate ($K_{500°C} = 21.5$ W $(m–k)^{-1}$ [31]) contributes to high levels of dilution, while the deposition current is directly proportional to the increase in dilution. However, since a single set of processing conditions and substrate (AISI 304) was used in this investigation, the changes in dilution shown in Fig. 9 are associated with the NiAl compound that formed in coatings.

The amount of heat released during the synthesis of NiAl depends on the amount of the aluminide that formed during solidification. Almeida et al. [23] demonstrated that the aluminum content in the Ni+Al powder mixture determines the level of dilution in the coatings: the greater the aluminum content in the mixture, the higher the dilution. Authors used Ni+Al powder mixtures with increasing aluminum content, from 15 to 50 wt.% Al and reported a progressive increase in dilution, ranging from 39 to 51%. This behavior is explained by a greater quantity of β-NiAl phase formed with increasing aluminum available in the deposited Ni+Al powder mixture a higher heat release at the solidification front during its synthesis, and hence a more significant impact of the plasma arc in substrate [23].

Extrapolating this analysis for the powder mixtures used in the present research, there is a proportional relationship between the amount of Al and the volume fraction

of NiAl compound formed. This is confirmed by chemical composition measured by EDS analysis on the transversal cross-section of the coatings. Aluminum content in coatings varied from 6.7 wt.% to 9.2 wt.% for C-90 and C-70 coatings, respectively (Fig. 10a). This smaller amount of NiAl in the C-90 coating is attributed to a loss of aluminum in the plasma arc, which is comparatively high.

Furthermore, it is also possible to establish a proportional relationship between the amount of NiAl compound formed and the measured dilution: the higher the volume fraction of β-NiAl phase, the higher the dilution (Fig. 10b). Figure 10c–f shows EDS analysis images, aiming to count the volume fraction of each phase. On the other hand, large amounts of the γ'-Ni_3Al phase in the C-90 coating (93.0%) account for the comparatively lower dilution measured in this coating (29.7% dilution), as shown in Fig. 10b and f. This behavior is associated to the comparatively low exothermic reaction of γ'-Ni_3Al phase synthesis (the enthalpy of formation of γ'-Ni_3Al is around −45 kJ/mol [32], which represents lower amounts of heat released during its formation compared to that of NiAl. Furthermore, the low amount of β-NiAl phase formed in the C-90 coating was not enough to affect the solidification behavior in the melt pool so that the dilution increases up to levels observed in C-0, C-50, and C-70 coatings.

It is important to highlight that even though the C-70 coating has the highest β-NiAl volume fraction (73.0%) and also the highest interaction with the substrate of all the coatings (45.09% dilution), it simultaneously exhibits the lowest γ-(Fe, Ni) volume fraction (27%). Thus, large amounts of iron diffusing from the substrate, did not only impact in the amount of the austenitic phase. A higher iron content is also found diluted in the β-NiAl phase, forming a (Ni, Fe)Al solid solution, as a consequence of the high solubility of iron in NiAl, as shown in the punctual EDS chemical analysis in Fig. 11, carried out in the main aluminide phases formed in each coating (β-NiAl phase for C-0, C-50, and C-70 coatings and γ'-Ni_3Al phase for C-90 coating).

This iron content within the β-NiAl phase has effects in the mechanical properties, which is evident as the average microhardness for C-0, C-50, and C-70 is at least 20% higher than that of the C-90 coating, that is, mostly formed by γ'-Ni_3Al (Fig. 12). Jin and Stephenson [33] pointed out that non-stoichiometric NiAl compositions can exhibit higher hardness than that of Ni_3Al. Hence, in Ni-rich compositions (55–60 at.% Ni) the hardness of NiAl can be up to 26% higher than that for Ni_3Al; This increase in hardness is even more severe for Al-rich compositions (45–49 at.% Ni) where the NiAl hardness can be 72 % higher than Ni_3Al [33]. Furthermore, iron in the (Ni, Fe)Al solid solution is known to increase the density of point defects [24, 29], which accounts for the changes in hardness profiles (Fig. 12).
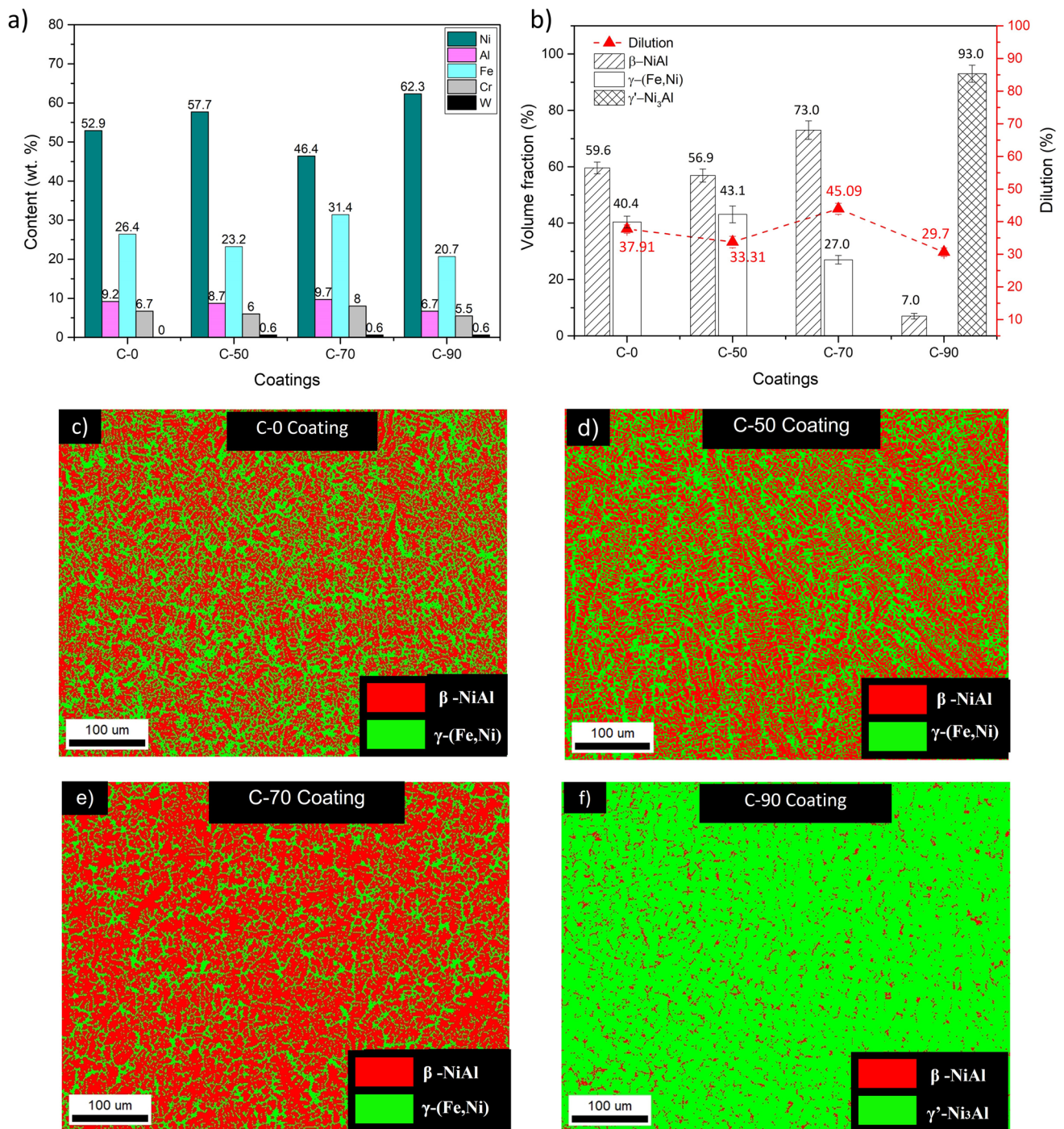
Fig. 10 Quantity and distribution of the phases (image analysis through EDAX OIM Analysis Software). **a** Chemical analysis of the coatings; **b** volume fraction and dilution of the coatings; **c** C-0 coating; **d** C-50 coating; **e** C-70 coating; **f** C-90 coating

In this sense, it is possible to predict that the larger amount of Fe in the C-70 coatings (Fig. 11) induces a higher density of point defects, resulting in a solid-solution-hardened Ni aluminide [24, 29], contributing to the highest measured hardness, 396.4 ± 8.3 HV, which is 12.6% higher than that of C-0 coating. Figure 12 also shows that the C-90

coating has the lowest average microhardness (289.4 ± 10.1 HV) as a consequence of a larger amount of γ'-Ni_3Al phase (with 93.0 %), combined with a low amount of hard β-NiAl phase (with only 7.0 %).

Not only do the characteristics of the aluminide compounds contribute to the understanding of these results
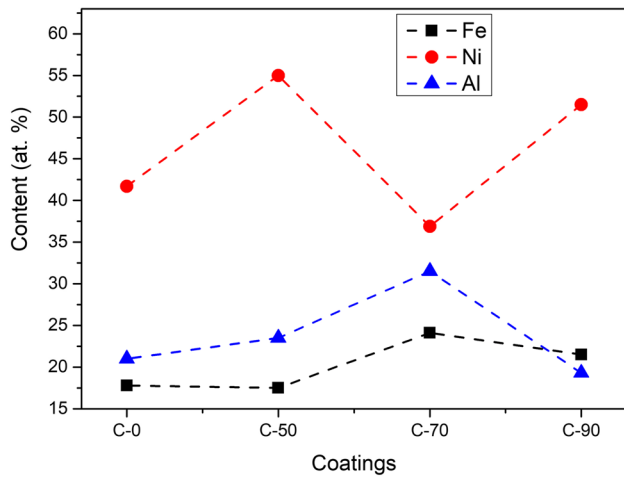
Fig. 11 Punctual EDS of β-NiAl phase (for C-0, C-50 and C-70 coatings) and γ'-Ni₃Al (for C-90 coating)
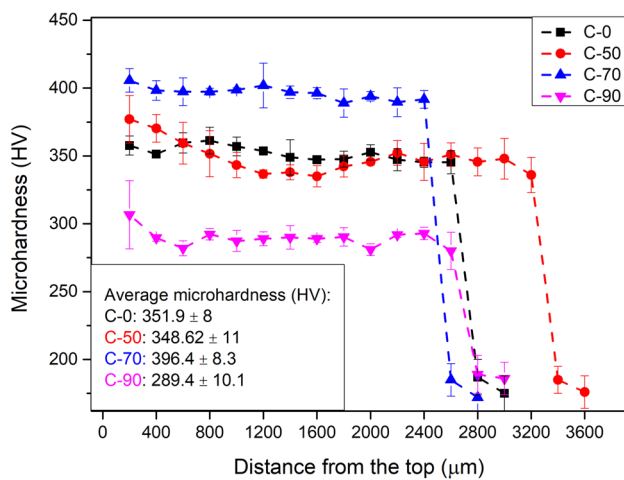

Fig. 12 Microhardness profile and average microhardness of the coatings

the volume fraction of each phase plays an important role: a larger volume fraction of hard NiAl phase in the C-70 coating combined with a lower volume fraction of ductile γ-(Fe, Ni) phase account for the highest average microhardness in the processed coatings. The hardness of β-NiAl-single-phase coatings (processed in similar conditions to those of this work) has been reported to be around 410 HV [24], which is considerably higher than that of the austenitic phase, ranging between 150 and 200 HV. Figure 12 shows that the average microhardness of C-0 and C-50 are quite similar, 351.9 ± 8 HV and 359.0 ± 8 HV, respectively, in agreement with similar volume fractions of β-NiAl and γ-(Fe, Ni) in both coatings.

Previous work [22] demonstrated that using all the Ni in the powder mixture (100% Ni) as carrier of the WC-NPs, compromises the synthesis of NiAl aluminide, as the WC-NPs form a liquid film surrounding the Ni particles, limiting the required interdiffusion between the molten Ni and Al in the plasma arc and leading to the loss of aluminum as powders cross the plasma and to the formation of Ni-rich aluminides, such as γ'-Ni₃Al. To better establish the interaction between powders in the plasma arc that accounts for the phases formed in coatings, Fig. 13a exhibits a representation of the interaction between elements when depositing Ni+Al powder mixtures without and with nanoparticle. The interaction between Ni and Al powders induces the synthesis of β-NiAl phase, while the deposition of powders on the melt pool in the austenitic substrate leads to the formation of the γ-(Fe, Ni) phase, as seen in the previous analysis.

This scenario changes when part of the Ni powders is used to carry NPs to process C-50, C-70, and C-90 coatings (Fig. 13b). The agglomeration of WC-NPs adhered to the surface of Ni particles forms a molten film that acts as a barrier to the interdiffusion of Ni and Al [22]. Hence, Ni particles without NPs ensure interdiffusion and the synthesis of the aluminide. Results show that a minimum of 30 wt.% Ni powders free to interact with Al in the plasma arc is required to process a sound NiAl-based coatings.

The behavior of powders in the plasma arc also allows us to understand the reported aluminum loss in coatings, which limited the formation of NiAl, changing the microstructure and microhardness. The measured loss of Aluminum in the C-90 coating is associated to a higher interference of WC-NPs in the synthesis of NiAl compound, as these nanoparticles covered the surface of 90% of the Ni particles in the powder mixture, leaving only 10% of Ni to directly react with aluminum. As the interdiffusion of Ni and Al is delayed by the melted film of NPs surrounding Ni particles, more aluminum was exposed to oxidation and/or vaporization, in the plasma arc as previously shown [22]. Lighter elements, such as aluminum, suffer higher losses during PTA-DED processing, due to vaporization [23].

Once the procedure to add NPs in Ni-Al powder mixtures while allowing to successfully obtain NiAl-based coatings by in situ synthesis was established, it is possible to assess the effects in microstructure. EBSD analysis shown in Fig. 14 reveals a 26% grain size reduction in the C-70 coating, compared to C-0 coating (without NPs), confirming this procedure to be a tool to customize microstructure and mechanical properties of coatings. The C-50 coating exhibits a small change in grain size with the addition of WC-NPs, as the average grain size is only 4.4% lower, compared to the C-0 coating. The white spaces among and around the

Fig. 13 Graphic representation of powder mixtures during PTA-DED processing. **a** Ni+Al powder mixture without nanoparticles; **b** Ni+Al powder mixtures containing 1 wt.% WC-NPs
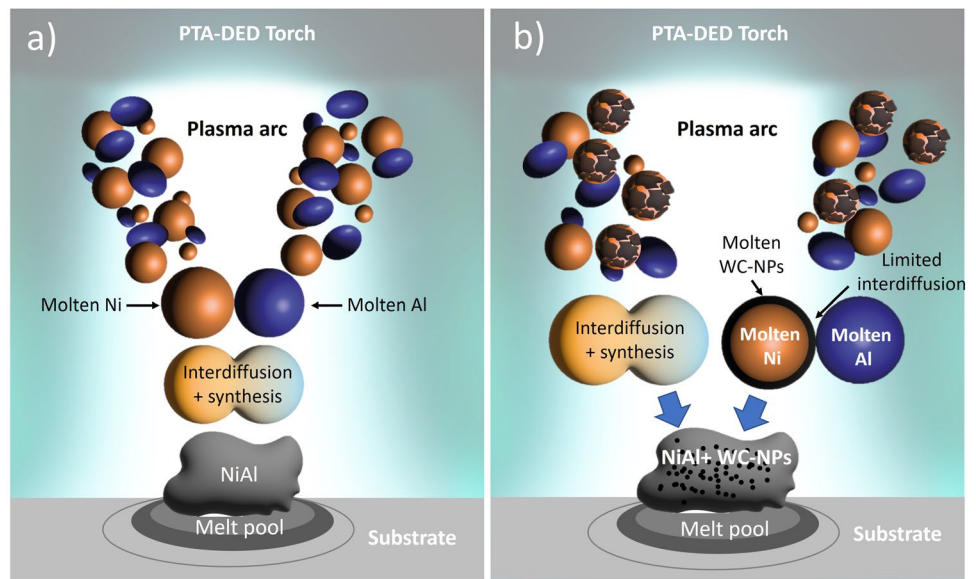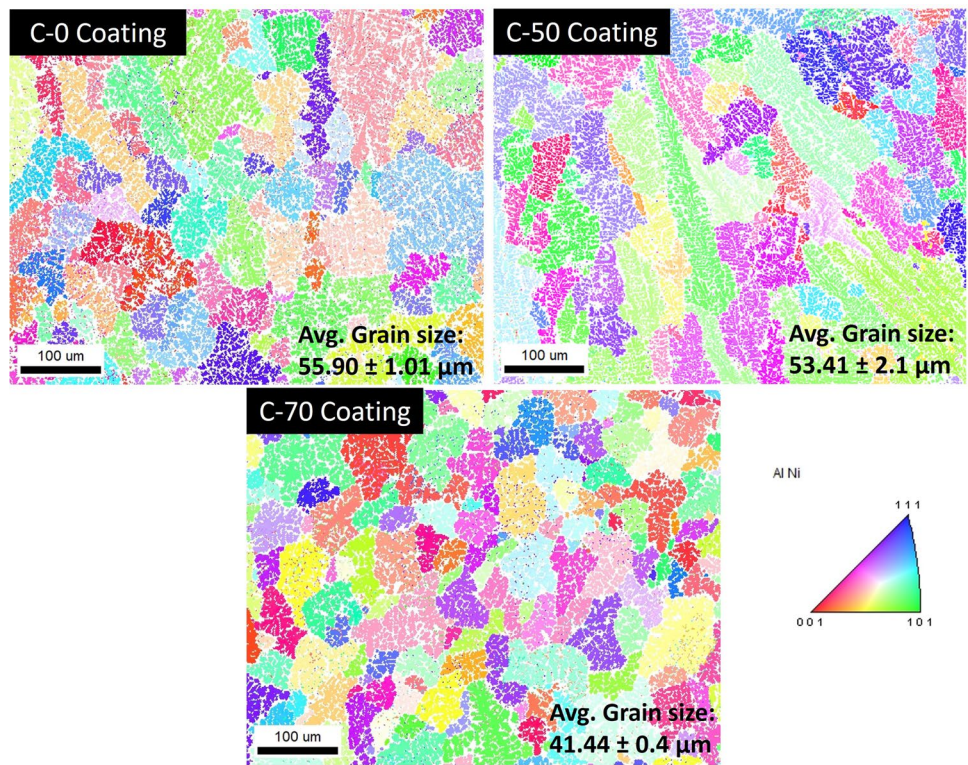

Fig. 14 EBSD analysis of the C-0, C-50, and C-70 coatings (white area refer to γ-(Fe, Ni) at the interdendritic regions)

NiAl grains in Fig. 14 represent the γ-(Fe, Ni) phase on the interdendritic regions.

The observed grain refinement may be associated to increase in nucleation and anchoring of grain boundaries [20]. However, these mechanisms associated to the observed grain refinement with the addition of WC-NPs should be further studied.

4 Conclusions

Under the conditions used in this research, to assess the impact of WC-NPs in the in situ synthesis of NiAl during the deposition of Ni+Al powder mixtures it is possible to conclude:

The method used to prepare Ni+Al powder mixture containing WC-NPs, consisting on the impregnation of the WC nanoparticles on a fraction of the Ni powders in the powder mixture (carriers), demonstrated to be suitable both to allow for the formation of NiAl compound and to transport these nanoparticles into the coatings. This is because there existed enough Ni molten particles to the interdiffusion with Al allowing to ignite the synthesis of the aluminide. Hence, the synthesis in situ of the β-NiAl phase was successfully achieved in NiAl-based coating containing 1 wt.% WC-NPs distributed in 50 and 70% of the Ni in the Ni+Al powder mixtures (C-50 and C-70 coatings, respectively).

The synthesis of NiAl compound in the C-90 coating was limited due to interferences to interdiffusion promoted by the impregnation of WC-NPs on 90% of the Ni (carriers) in the Ni+Al powder mixture, leading to the loss of Al and the formation of mostly Ni$_3$Al. Hence, a minimum of 30 wt.% Ni powders free to interact with Al in the plasma arc is required to process a sound NiAl-based coatings.

In (Ni, Fe)Al solid solution substitutional iron promoted the formation of constitutional point defects in the NiAl crystal structure of C-0, C-50, and C-70 coatings, accounting for an increase in the microhardness of these coatings of at least 20% higher to that of C-90 coating, formed mostly by γ'-Ni$_3$Al. This increase in microhardness is more evident in the C-70 coating due to a higher iron content and also the highest β-NiAl volume fraction of all the processed coatings.

The addition of WC-NPs induced to a grain refinement, which was more evident in the C-70 coating with approximately 26% grain size reduction compared with the C-0 coating.

Declarations

Ethics approval This is an original work that has not been published or considered for publication elsewhere in any form or language.

Consent to participate Not applicable

Consent for publication Not applicable

Competing interests The authors declare no competing interests.

References

1. Hou S, Liu Z, Liu D, Ma Y (2012) Oxidation behavior of NiAl-TiB2 coatings prepared by electrothermal explosion ultrahigh speed spraying. Physics Procedia 32:71–77

2. Scheppe F, Sahm PR, Hermann W, Paul U, Preuhs J (2002) Nickel aluminides: a step toward industrial application. Mater Sci Eng: A 329:596–601

3. Noebe RD, Bowman RR, Nathal MV (1996) The physical and mechanical metallurgy of NiAl. In: Stolof NS, Sikka VK (eds) Physical metallurgy and processing of intermetallic compounds. Chapman & Hall, New York, pp 212–296

4. Hyjek P, Sulima I, Jaworska L (2019) Application of SHS in the Manufacture of (NiAl/Ni 3 Al)/TiB 2 composite. Metall Mater Trans A 50:3724–3735

5. Bochenek K, Basista M (2015) Advances in processing of NiAl intermetallic alloys and composites for high temperature aerospace applications. Prog Aerosp Sci 79:136–146

6. Wu Q, Li S, Ma Y, Gong S (2013) Study on behavior of NiAl coating with different Ni/Al ratios. Vacuum 93:37–44

7. Fan GH, Wang QW, Du Y, Geng L, Hu W, Zhang X, Huang YD (2014) Producing laminated NiAl with bimodal distribution of grain size by solid–liquid reaction treatment. Mater Sci Eng: A 590:318–322

8. Schulson EM, Barker DR (1983) A brittle to ductile transition in NiAl of a critical grain size. Scripta Metall 17:519–522

9. Cheng T (1992) Improvement of mechanical properties of nickel-rich NiAl at room temperature. Scripta Metall et Mater 27(6):771–776

10. Kaplin C, Ivanov R, Paliwal M, Jung IH, Brochu M (2014) The effect of nanostructure on the oxidation of NiAl. Intermetallics 54:209–217

11. Matsuura K, Kudoh M (1997) Grain refinement of combustion-synthesized NiAl by addition of ceramic particles. Mater Sci Eng: A 239:625–632

12. Kou SQ, Gao YL, Song W, Zhao HL, Guo YB, Zhang S, Yang HY (2021) Compression properties and work-hardening behavior of the NiAl matrix composite reinforced with in situ TaC ceramic particulates. Vacuum 186:110035

13. Doi Y, Matsuki K, Akimoto H, Aida T, Ochiai S (2001) Grain refinement and high strain rate superplasticity in (γ'+ β) two phase nickel aluminides reinforced with TiC particles. Nippon Kinzoku Gakkaishi/J Japan Inst Metals 65(5):449–457

14. Awotunde MA, Ayodele OO, Adegbenjo AO, Okoro AM, Shongwe MB, Olubambi PA (2019) NiAl intermetallic composites—a review of processing methods, reinforcements and mechanical properties. Int J Adv Manuf Technol 104:1733–1747

15. Goudarzi A, Lalianpour A, Mehrizi MZ, Beygi R (2019) Fabrication of NiAl–Al2O3-WC nanocomposite by mechanical alloying and subsequent heat treatment. Ceram Int 45(15):19049–19054

16. Molina-Claros J, Hdz-García HM, Alvarez-Vera M, Pech-Canul MI, Muñoz-Arroyo R, García-Vázquez F, … Díaz-Guillen JC

(2017) Characterisation of PTA processed overlays without and with WC nanoparticles. Surf Eng 33(11), 857-865.

17. Acevedo-Dávila JL, Muñoz-Arroyo R, Hdz-García HM, Martinez-Enriquez AI, Alvarez-Vera M, Hernández-García FA (2017) Cobalt-based PTA coatings, effects of addition of TiC nanoparticles. Vacuum 143:14–22

18. Deuis RL, Yellup JM, Subramanian C (1998) Metal-matrix composite coatings by PTA surfacing. Compos Sci Technol 58(2):299–309

19. DebRoy T, Wei HL, Zuback JS, Mukherjee T, Elmer JW, Milewski JO, ... Zhang W (2018) Additive manufacturing of metallic components–process, structure and properties. Prog Mater Sci 92, 112-224.

20. Bond D, Lussoli RJ, Neto JB, D'Oliveira ASCM (2018) Co-based superalloy (Stellite 6) powder with added nanoparticles to be molten by PTA. Soldagem & Insp 25:1–11

21. Prass GS, d'Oliveira ASC (2023) Processing and characterization of AISI 316L coatings modified with Cu and CuO nanoparticles. Surf Coat Technol 461:129465

22. Abreu-Castillo HO, Bueno BP, d'Oliveira ASC (2022) In situ processing aluminide coatings with and without tungsten carbide. Int J Adv Manuf Technol 119(1–2):477–488

23. Almeida VB, Takano EH, Mazzaro I, D'Oliveira ASCM (2011) Evaluation of Ni–Al coatings processed by plasma transferred arc. Surf Eng 27(4):266–271

24. Brunetti C, Pintaude G, d'Oliveira ASCM (2014) The influence of Fe content on the mechanical properties of NiAl coatings processed in-situ. J Mater Eng Perform 23:3934–3940

25. Yaedu AE, D'Oliveira ASCM (2005) Co based alloy PTA hardfacing with different dilution levels. Mater Sci Technol 21(4):459–66

26. Zhang Z, Huang X, Yao P, Xue J (2021) A new method for weld dilution calculation through chemical composition analysis. Metals 11(1):131

27. Okamoto H (2004) Al-Ni (Aluminum-Nickel). J Ph Equilibria and Diffus 25:394

28. Cotton JD, Noebe RD, Kaufman MJ (1993) Ternary alloying effects in polycrystalline {beta}-NiAl. Los Alamos National Lab., New Mexico, United States. https://www.osti.gov/servlets/purl/10157276-1U5Ani/. Accessed 30/07/2024

29. Pike LM, Chang YA, Liu CT (1997) Solid-solution hardening and softening by Fe additions to NiAl. Intermetallics 5(8):601–608

30. Breuer J, Grün A, Sommer F, Mittemeijer EJ (2001) Enthalpy of formation of B2-Fe $1–x$ Al x and B2-(Ni, Fe) $1–x$ Al x. Metall Mater Trans B 32:913–918

31. Chu TK, Ho CY (1978) Thermal conductivity and electrical resistivity of eight selected AISI stainless steels. Thermal Conductivity 15:79–104

32. Sikka VK (1996) Processing of aluminides. Physical metallurgy and processing of intermetallic compounds. Springer, US, Boston, MA, pp 561–604

33. Jin JH, Stephenson DJ (1998) The sliding wear behaviour of reactively hot pressed nickel aluminides. Wear 217(2):200–207